PCCP

PAPER

View Article Online
View Journal | View Issue

Cite this: *Phys. Chem. Chem. Phys.*, 2016, **18**, 18312

Electronic structure engineering of various structural phases of phosphorene†

Sumandeep Kaur,*[a] Ashok Kumar,*[b] Sunita Srivastava*[a] and K. Tankeshwar*[c]

We report the tailoring of the electronic structures of various structural phases of phosphorene (α-P, β-P, γ-P and δ-P) based homo- and hetero-bilayers through in-plane mechanical strains, vertical pressure and transverse electric field by employing density functional theory. In-plane biaxial strains have considerably modified the electronic bandgap of both homo- and hetero-bilayers while vertical pressure induces metallization in the considered structures. The γ-P homo-bilayer structure showed the highest ultimate tensile strength (UTS ∼ 6.21 GPa) upon in-plane stretching. Upon application of a transverse electric field, the variation in the bandgap of hetero-bilayers was found to be strongly dependent on the polarity of the applied field which is attributed to the counterbalance between the external electric field and the internal field induced by different structural phases and heterogeneity in the arrangements of atoms of each surface of the hetero-bilayer system. Our results demonstrate that the electronic structures of the considered hetero- and homo-bilayers of phosphorene could be modified by biaxial strain, pressure and electric field to achieve the desired properties for future nano-electronic devices.

Received 24th February 2016,
Accepted 8th June 2016

DOI: 10.1039/c6cp01252c

www.rsc.org/pccp

1. Introduction

The exquisite electronic properties of graphene, which include the presence of massless Dirac fermions, high carrier mobility, excellent electrical and thermal conductivity, have won the Nobel prize 2010 for its discoverers.[1] However, the lack of the bandgap in graphene limits its applications in nano- and optoelectronics, which has therefore triggered the interest of scientists in graphene-alternatives that currently lead to the emergence of a number of 2D materials such as silicene, germanene, hexagonal boron nitride (h-BN) and transition metal dichalcogenides (TMDs).[2–4] Silicene and germanene are semi-metallic in nature similar to graphene, while hexagonal boron nitride is an insulator and TMDs are semiconductors.[5,6]

Recently, layered phosphorous, which is a new member of the family of 2D materials, has gathered a great deal of attention because of the possibility of mechanical exfoliation of layered bulk black phosphorous (BP) to yield few layer phosphorene[7] with a sizable bandgap of ∼1 eV.[8] Note that the carrier mobility of phosphorene is ∼1000 $cm^2 V^{-1} s^{-1}$,[9,10] which is considerably higher than the value of ∼200 $cm^2 V^{-1} s^{-1}$ obtained for 2D layered TMDs. Monolayer black phosphorene is also found to exhibit giant phononic anisotropy that can be tuned by strain and there is also an orientation dependent anisotropy in the interlayer coupling of few-layer phosphorene.[11] The first principles calculations reveal that not only black phosphorene (α-P), but also other phases such as blue-phosphorene (β-P),[12] gamma-phosphorene (γ-P)[13] and delta-phosphorene (δ-P)[13,14] possess energetically and thermodynamically stable structures which require greater attention. A very recent study has predicted another four monolayer phosphorous allotropes with energetically stable structures *i.e.*, ε-P, ζ-P, η-P and θ-P and through their hybridization another five energetically favorable structures can be formed.[15] Although various methods like cleavage with tape, liquid-phase exfoliation, plasma-assisted fabrication[16] and chemical vapor deposition[17] have been used to fabricate single or few layer black phosphorous (α-P) the experimental realization of the other stable allotropes of phosphorene and their multi-layer structure is missing in the literature. Experimental results on van der Waals heterostructures have not been reported probably due to poor control in stacking the heterostructures. Thus, sincere and consecrated efforts are required from the experimentalists of the materials and chemistry community to carry out experiments for fabricating the heterostructures of various allotropes of phosphorene.

The possibility of band structure engineering by the formation of heterostructures based on 2D materials to develop novel devices opens up a new area of research.[18,19] The layered structures of various phases of phosphorene exhibit strong covalent bonding which holds the in-plane atoms, while the

[a] *Department of Physics, Panjab University, Chandigarh 160014, India. E-mail: dusuman0015@gmail.com, sunita@pu.ac.in*
[b] *Centre for Physical Sciences, School of Basic and Applied Sciences, Central University of Punjab, Bathinda, 151001, India. E-mail: ashok.1777@yahoo.com*
[c] *Department of Physics, Guru Jambheshwar University of Science and Technology, Hisar, 125001, Haryana, India. E-mail: tkumar@gjust.org*

† Electronic supplementary information (ESI) available. See DOI: 10.1039/c6cp01252c

vertically stacked layers are held together by weak van der Waal forces. Due to the layered nature, phosphorene offers the opportunity to fabricate devices based on vertical heterostructures for novel nano- and opto-electronic applications *e.g.* the h-BN/phosphorene heterostructure shows the possibility to assist experimentalists in identifying different structural phases of phosphorus;[20] the phosphorene/graphene heterostructure shows ohmic as well as rectifying character[21] that makes it a potential electrode material in Li batteries.[22] Both h-BN as well as graphene are found to effectively prevent the degradation of phosphorene while retaining its pristine electronic properties intact and they are also able to tune its carrier dynamics and optical properties;[23] phosphorene/MoS_2 acts as a p–n diode[24] with a very high photo detection power and a CMOS inverter[25] with the possibility to be used as a novel channel material for future electronic applications; metal/BP interfaces such as Cu/BP form ohmic contact while Zn/BP and In/BP form Schottky contacts[26] in devices, *etc.*

Furthermore, the electronic properties of nanomaterials including heterostructures can be modulated by applying an external electric field, in-plain mechanical strains and vertical pressures which are considered to be novel and promising methods to modify the fundamental bandgap of the 2D materials.[27–29] For characterizing the inhomogeneous distribution of strain and its measurements, the strain-induced frequency shifts and variation in energy spacing between the peaks of the characteristic vibrational mode in Raman spectra can be analyzed. Fei and Yang have used this method to quantify arbitrary strain distributions in monolayer black phosphorene.[30] Note that the tuning of the fundamental direct bandgap of black phosphorous with a number of layers, electric field and in-plane layer compression or expansion makes few layer phosphorene a promising candidate for many applications *e.g.* as a photodetector in the visible to infrared light range,[31,32] as a novel thermoelectric material[33,34] with possible applications in portable electronic systems, as a gas sensor,[35] in advanced battery applications,[36] *etc.*

Although black phosphorene (α-P) has already been studied in the literature less attention has been paid to the other three energetically and thermodynamically favorable structural phases *i.e.* β-P, γ-P and δ-P. Therefore, in the present paper, we have looked into the details of the electronic properties of vertical heterostructures (homo- and hetero-bilayers) of the various structural phases of phosphorene by taking into consideration the effect of the external electric field, in-plane strains and vertical pressure.

2. Computational method

All the calculations have been performed by using the SIESTA simulation package.[37] The norm-conserving Troullier Martins pseudo potential in fully separable Kleinman and Bylander form has been used to treat the electron–ion interactions.[38] The exchange and correlation energies have been treated within both GGA-PBE and van der Waals (vdW)-DRSLL functionals.[39] The Kohn Sham orbitals were expanded as a linear combination of numerical pseudo atomic orbitals using a split-valence double zeta basis set with polarization functions (DZP). Throughout geometry optimization, the confinement energy of numerical pseudo-atomic orbitals is considered to be 0.01 Ry. Minimization of energy was carried out using the standard conjugate-gradient (CG) technique. Structures were relaxed until the forces on each atom were less than 0.01 eV $Å^{-1}$. The Monkhorst–Pack scheme is used to sample the Brillouin zone using a $10 \times 10 \times 1$ mesh for the calculations based on hetero-bilayers and a $30 \times 30 \times 1$ mesh for homo-bilayers. The spacing of the real space used to calculate the Hartree exchange and correlation contribution of the total energy and Hamiltonian was 450 Ry. A vacuum region of about 20 Å perpendicular to the 2D plane has been used in calculations to prevent the superficial interactions between the periodic images.

3. Results and discussion

The two dimensional (2D) crystal structures of α-P, γ-P and δ-P have a rectangular primitive cell with 4, 4 and 8 atoms respectively, while β-P possess 2 atoms in the hexagonal primitive cell.[13] All the considered phases of monolayer phosphorene *i.e.* α-P, β-P, γ-P and δ-P, are semiconductors with the calculated bandgap values of 1.12 eV, 2.05 eV, 0.79 eV and 0.62 Ev, respectively. The bandgap values calculated using the GGA-PBE functional are 0.94 eV, 2.02 eV, 0.55 eV and 0.29 Ev, respectively, for α-P, β-P, γ-P and δ-P. Our vdW-DRSLL results are in better agreement with the experimental values obtained for α-P (1.45 eV).[25] The valence band maximum (VBM) and conduction band minimum (CBM) in α-P and δ-P lie on the same high symmetry point making them direct bandgap semiconductors while β-P and γ-P are indirect bandgap semiconductors (Fig. S1 of the ESI†). Note that the Brillouin zone of α-P, γ-P and δ-P is rectangular with a high symmetry path S-Y-Γ-X-S while β-P possess a hexagonal Brillouin zone with a high symmetry path K-Γ-M-K. The states around the Fermi level for all the phases are mainly contributed by the p-orbitals of P atoms.

3.1. Homo-bilayers of phosphorene

Similar to graphene, the bilayers of phosphorene can have two different types of stacking pattern *i.e.* AB and AA. The crystal structure of homo-bilayers (*i.e.* two layers with the same structural phase) with a primitive cell is shown in Fig. 1. Homo-bilayers of α-P, β-P, γ-P and δ-P possess 8, 4, 8 and 16 atoms, respectively, in 1×1 supercells. Our total energy calculations reveal AB-stacking to be most favorable for the α-P bilayer, while β-P (hexagonal unitcell), γ-P and δ-P bilayers prefer the AA-stacking pattern. The difference in total energy between two different types of stacking in α-P, β-P, γ-P and δ-P bilayers is found to be 0.09 meV per atom, 0.02 meV per atom, 4 meV per atom and 2 meV per atom, respectively. Note that previous first principles calculations of α-P also predict the AB-stacking pattern to be most favorable.[40] In another report,[41] AA-stacking marginally prefers over AB-stacking in β-P bilayers which is consistent with our prediction. Homo-bilayers of α-P show a

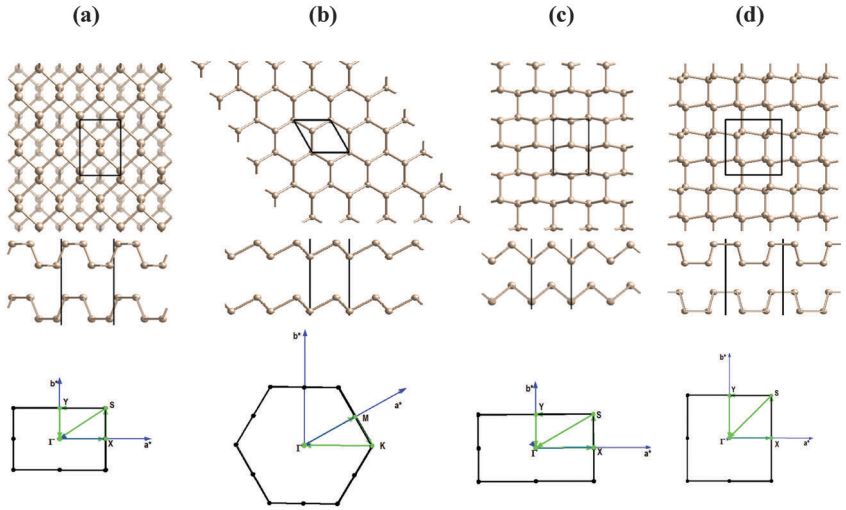

Fig. 1 Top and side view of homo-bilayers (a) α-P/α-P, (b) β-P/β-P (c) γ-P/γ-P and (d) δ-P/δ-P. (1 × 1) unit cell is also indicated by solid lines. Light colored atoms in top views represent the underneath layer. α-P bilayers stabilized into the AB-stacked pattern while β-P, γ-P and δ-P prefers AA-stacking. In the Brillouin zone, a* and b* along the blue lines indicate reciprocal lattice vectors and the green lines show the path chosen for Brillouin zone sampling.

direct bandgap of 0.92 eV which is in good agreement with other reported values in the literature[42] whereas β-P (hexagonal unitcell) is an indirect bandgap semiconductor with a bandgap value of 1.49 eV (Fig. 2 and Table 1). Our van der Waals functional based calculations indicate the γ-P bilayer to be an indirect bandgap semiconductor with a bandgap value of 0.29 eV (Fig. 2(c)) while our GGA-PBE calculations predict metallic character of γ-P (Fig. S2(a) of the ESI†) as also reported in the literature.[13] Using the vdW-DRSLL functional, we find the δ-P bilayer to be a direct bandgap semiconductor with a bandgap value of 0.38 eV while our GGA-PBE calculations predict Dirac cone like character at the Fermi level of the δ-P bilayer (Fig. 2(d) and Fig. S2(b) of the ESI†), which mainly consists of the 3p orbitals of P atoms. Note that four layer thick black phosphorene[43] and

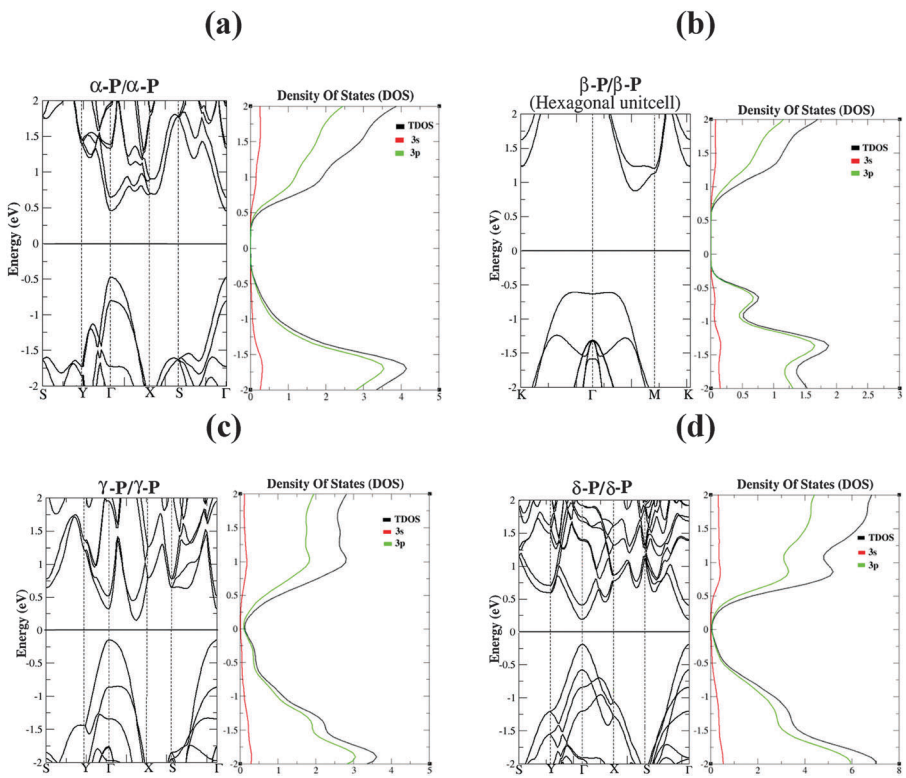

Fig. 2 The electronic band structure and density of states of the homo-bilayers (a) α-P (b) β-P (c) γ-P and (d) δ-P.

Table 1 Lattice constants (a, b), supercells, the number of atoms per unit cell (N), interlayer distance (R), binding energy per atom (E_b) and bandgap (E_g) of the considered homo-bilayers

Parameter	α-P/α-P		β-P/β-P (hexagonal cell)		γ-P/γ-P		δ-P/δ-P	
Functional	GGA-PBE	vdW	GGA-PBE	vdW	GGA-PBE	vdW	GGA-PBE	vdW
a, b (Å)	3.35	3.42	3.32	3.42	3.41	3.41	5.43	5.81
	4.47	4.84	3.32	3.42	5.30	5.67	5.38	5.67
Supercell	1 × 1	1 × 1	1 × 1	1 × 1	1 × 1	1 × 1	1 × 1	1 × 1
N	8	8	4	4	8	8	16	16
R (Å)	3.25	3.78	3.49	3.78	2.31	3.73	3.37	3.82
E_b (meV per atom)	31	50	30	57	67	61	34	51
E_g (eV)	0.48	0.92	1.30	1.49	0	0.29	0	0.38

hydrogenated blue phosphorene[44] are also found to possess graphene-like Dirac cone features. However, it has been well-known that the GGA-PBE cannot accurately describe the vdW interaction and even for the case of mono and bilayer α-P, it is found to underestimate the bandgap.[42] So, for further calculations of van der Waals bilayers, we have used the vdW-DRSLL functional that incorporates the vdW interactions.

Our calculated binding energy per atom of homo-bilayers is found to be of the order of a few meV (Table 1) which indicates weak van der Waals interactions between the layers. The binding energy (E_b) per atom was calculated as: $E_b = [E - (E_1 + E_2)]/N$, where E_1 and E_2 are the total energy of isolated layers, E is the total energy of bilayer system and N is the total number of atoms in the supercell. In contrast to the monolayer, the electronic band structure of bilayers shows reduction in the electronic bandgap which is attributed to the splitting of energy levels due to interlayer interactions (Fig. S1, ESI† and Fig. 2).[42] In order to gain further insight into the interlayer interactions, the charge density difference has been calculated which shows the accumulation of charge between the layers (Fig. S3 of the ESI†) which results in the reduction of the bandgap in bilayers. Here the charge density difference profile is obtained as $\Delta\rho = \rho - (\rho_1 + \rho_2)$, where ρ is charge density of the bilayer while ρ_1 and ρ_2 are charge densities of isolated monolayers.

3.2. Hetero-bilayers of phosphorene

Now we consider the four possible commensurable vertical hetero-bilayer structures *i.e.* α-P/β-P, γ-P/δ-P, γ-P/β-P and δ-P/β-P (Fig. 3) of four structural phases of phosphorene. The commensurable bilayer structures are constructed in order to minimize the interfacial strain between the layers of different phases. For example, the supercell of α-P/β-P (Fig. 3(a)) consists of 5 × 1 unit cells of monolayer α-P vertically stacked over 4 × 1 unit cells of monolayer β-P, that results in ~2.2% lattice mismatch between the vertically stacked layers. Similarly, the choice of 5 × 1/3 × 1 unit cells in γ-P/δ-P (Fig. 3(b)), 1 × 1/1 × 1 unit cells in γ-P/β-P (Fig. 3(c)) and 3 × 1/5 × 1 unit cells of δ-P/β-P (Fig. 3(d)), produce a minimum lattice mismatch of about 2.7% in γ-P/δ-P, 4.6% in γ-P/β-P and 6.5% in δ-P/β-P (Table 2). Note that bilayer α-P twisted by an angle of 2.5° has been found to possess AA, AB and AC stacking regions within its Moire pattern.[45] Our bilayer systems particularly those with

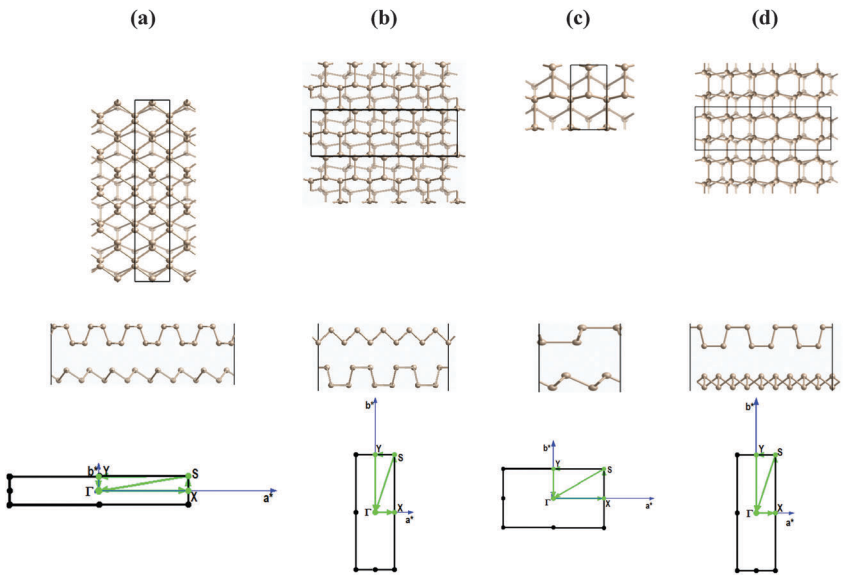

Fig. 3 Top and side view of the hetero-bilayers (a) α-P/β-P, (b) γ-P/δ-P, (c) γ-P/β-P and (d) δ-P/β-P. Light colored atoms in top view indicate the underneath layer. In the Brillouin zone, a* and b* along the blue lines indicate reciprocal lattice vectors and the green lines show the path chosen for Brillouin zone sampling.

Table 2 Lattice constants (a, b), supercells, the number of atoms per unit cell (N), interlayer distance (R), binding energy per atom (E_b) and bandgap (E_g) of the considered hetero-bilayers

Parameter	α-P/β-P		γ-P/δ-P		γ-P/β-P		δ-P/β-P	
Functional	GGA-PBE	vdW	GGA-PBE	vdW	GGA-PBE	vdW	GGA-PBE	vdW
a, b (Å)	3.34 22.55	3.41 24.18	16.47 5.42	17.46 5.67	3.31 5.73	3.41 5.91	16.47 5.42	17.46 5.67
Supercell	5 × 1(α-P) 4 × 1(β-P)	5 × 1(α-P) 4 × 1(β-P)	5 × 1(γ-P) 3 × 1(δ-P)	5 × 1(γ-P) 3 × 1(δ-P)	1 × 1(γ-P) 1 × 1(β-P)	1 × 1(γ-P) 1 × 1(β-P)	5 × 1(β-P) 3 × 1(δ-P)	5 × 1(β-P) 3 × 1(δ-P)
N	36	36	44	44	8	8	44	44
R (Å)	3.50	3.8	3.10	3.7	3.50	3.8	3.50	3.8
E_b (meV per atom)	29	53	36	53	29	55	30	52
E_g (eV)	0.85	1.32	0.13	0.24	0.97	1.02	0.08	0.36

a large lattice mismatch (γ-P/β-P and δ-P/β-P) may show the possibility of the formation of the Moire pattern with different stacking regions and in that case the bandgaps would possibly be the lowest of different stacking styles.

Note that, in order to make the heterostructure of β-P with other allotropes, its rectangular unit cell is used to obtain the commensurable lattice. We have calculated the lattice constant a = 3.41 Å and b = 5.91 Å for the rectangular unit cell of β-P. The bandgap value of 2.05 eV (Fig. S1 of ESI†) is in line with the value calculated with the hexagonal unit cell. The favorable stacking pattern is AB in the bilayer of β-P (rectangular unit cell), however the energy difference between the total energy of both the stacking patterns is negligibly small (0.5 meV per atom). Fig. S4 and S5 of the ESI† show the stacking pattern and the band structure of β-P in the rectangular unit cell with a bandgap value of 1.46 eV.

The binding energy per atom in the considered hetero-bilayer structures is of the order of a few meV which indicates weak van der Waals interactions between the hetero-bilayers. It is interesting to note that the band structures of considered hetero-bilayers have an indirect bandgap in nature except γ-P/δ-P which shows a direct bandgap (Fig. 4) while their monolayer counterparts *i.e.*, α-P and δ-P have direct bandgaps and β-P and γ-P have indirect bandgaps (Fig. S1, ESI†). The calculated charge density difference profile (Fig. S6 of the ESI†) show charge redistributions between the layers that result in a smaller energy gap in the electronic structure.

3.3. Ultimate tensile strength of homo- and hetero-bilayers

To examine the in-plane flexibility or tensile strength of both homo- and hetero-bilayers, we have applied an in-plane

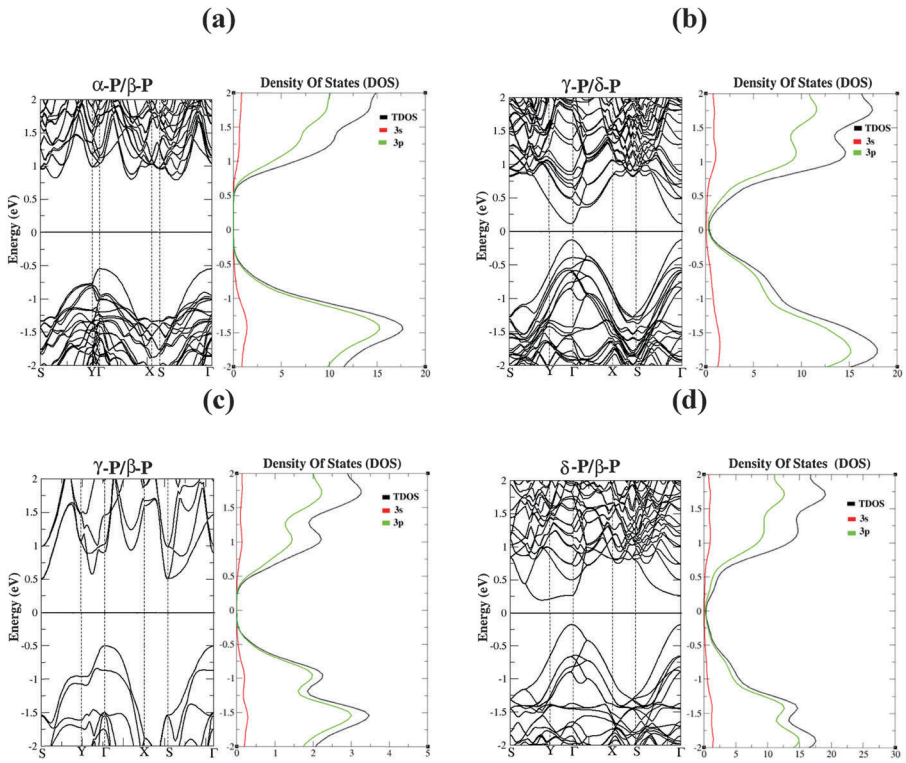

Fig. 4 The electronic band structure and the corresponding total and partial density of states of hetero-bilayers (a) α-P/β-P and (b) γ-P/δ-P, (c) γ-P/β-P and (d) δ-P/β-P.

stretching strains along x and y directions simultaneously. The mechanical strain, $e = \Delta a/a_0$, was applied in small steps where a_0 is the equilibrium lattice constant and Δa is the change in lattice constant obtained after deformation of the lattice.[46] The maximum stress that a bilayer system can withstand before breaking gives its ultimate tensile strength (UTS). The value of UTS is the point at which the slope of the strain–stress curve becomes zero. The strain–stress can be determined by calculating the stress tensor components in response to the strain tensor. The stress tensor is defined as a positive derivative of total energy with respect to the strain tensor.[37]

Upon application of biaxial strain, the stress obtained along x and y directions in all the considered structures is shown in Fig. 5. The stress–strain curves for hetero-bilayers were obtained after subtracting the stress introduced due to lattice mismatch at the zero strain value. The values of strain at which the ultimate tensile strength (UTS) is obtained for x and y directions and the UTS values are listed in Table 3. The highest UTS values among homo-bilayers are found for the γ-P structural phase where the UTS values of 6.21 GPa and 4.47 GPa along x and y directions, respectively, have been obtained with respective ultimate strain values of 32% and 22%. Note that the UTS and ultimate strain value of β-P homo-bilayers in the rectangular unit cell have been calculated as 4.84 GPa and 26% along the x as well as along the y direction (Fig. S7 of the ESI†). Similarly, the highest UTS values among hetero-bilayers are obtained for γ-P/β-P (Table 3). We have found UTS values in the range of 2.8–6.2 GPa for considered homo- and hetero-bilayers. The differences in stress values along x and y directions may be attributed to the structural differences along the two directions or the differences in lattice constants along x and y directions.

3.4. Bandgap as a function of in-plane strain

Now we consider the effect of biaxial tensile strain on the bandgap of considered homo- and hetero-bilayers (Fig. 6). The bandgap of the homo-bilayer (in the case of α-P, γ-P and δ-P) initially increases up to 6%, 4% and 8% applied strain values respectively while upon further increasing the strain the bandgap decreases to 0 eV at 34%, 14% and 34% of strain respectively for α-P, γ-P and δ-P (Fig. 6(a)). But strain values at which the metallization is obtained in α-P and δ-P are higher than their respective UTS values. In the β-P homo-bilayer, the bandgap decreases with the application of strain with the

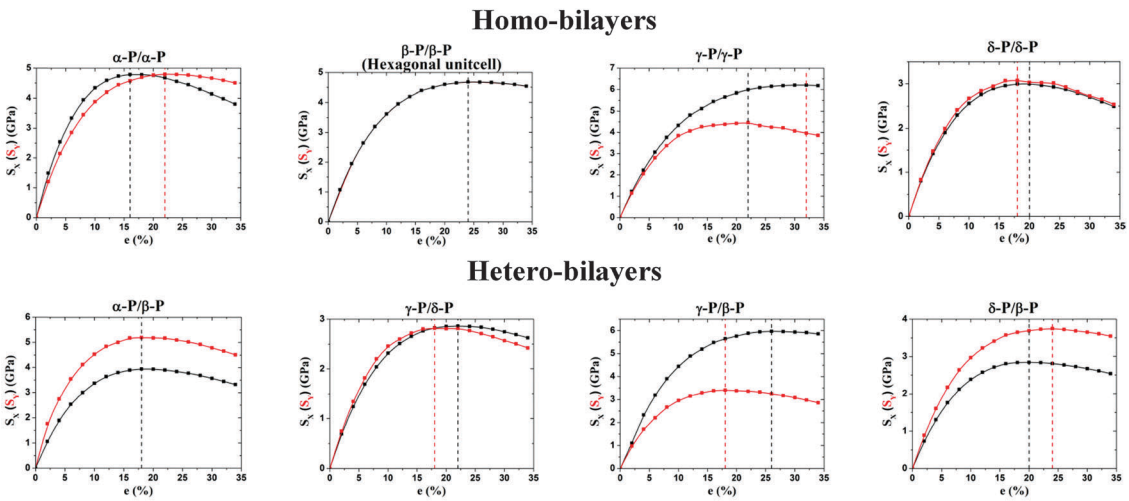

Fig. 5 The strain–stress curves of the considered homo- and hetero-bilayers of various structural phases of phosphorene. Black/red color shows stress S_x/S_y along the x/y direction in response to biaxial strain (e). The vertical lines indicate the ultimate strain value at which the slope of the strain–stress curve becomes zero.

Table 3 Ultimate tensile stress (UTS) S_x and S_y, along x and y directions, the corresponding ultimate in-plane biaxial strains (e_x and e_y), ultimate pressure (P_m) and interlayer distance (d_m) at which metallization occurs in the considered bilayer systems

Parameter	α-P/α-P		β-P/β-P (hexagonal unit cell)		γ-P/γ-P		δ-P/δ-P		α-P/α-P		γ-P/δ-P		γ-P/β-P		δ-P/β-P	
Functional	GGA-PBE	vdW	GGA-PBE	vdW	GGA-PBE	vdW	GGA-PBE	vdW	GGA-PBE	vdW	GGA-PBE	vdW	GGA-PBE	vdW	GGA-PBE	vdW
UTS (GPa)																
S_x	6.77	4.79	5.71	4.68	8.27	6.21	4.09	3.00	6.26	5.19	3.84	2.86	6.96	5.98	4.01	2.85
S_y	5.89	4.80	5.71	4.68	6.64	4.47	4.16	3.08	6.52	3.95	3.49	2.82	3.99	3.41	4.92	3.75
e_x (%)	18	16	26	24	30	32	20	20	19	18	23	22	28	26	21	20
e_y (%)	19	22	26	24	18	22	20	18	23	18	17	18	19	18	23	24
P_m (GPa)	2.82	7.11	1.74	4.77	—	2.0	—	4.42	7.00	9.62	—	—	6.04	8.18	7.73	11.34
d_m (Å)	2.69	2.4	2.50	2.5	—	3.0	—	3.0	2.38	2.3	—	—	2.3	2.3	2.4	2.3

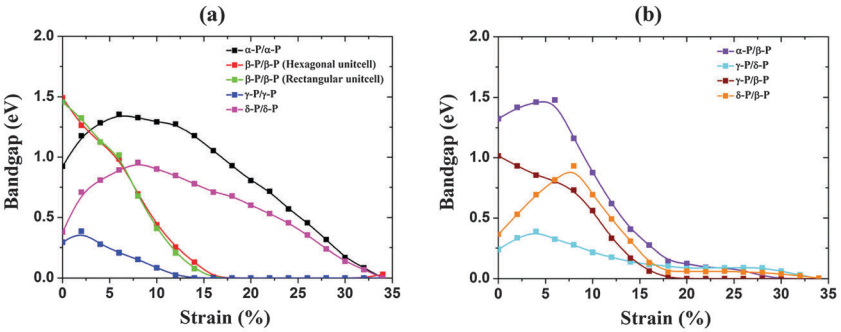

Fig. 6 The bandgap as a function of biaxial strain in (a) homo-bilayers and (b) hetero-bilayers of various structural phases of phosphorene.

occurrence of a semiconductor-to-metal transition at 16% value of strain. Also, there occurs a direct to indirect bandgap transition at 4% (4%) and then indirect to direct bandgap transition at 23% (26%) of strain value in the case of the α-P (δ-P) bilayer. However, in the case of the β-P (γ-P) bilayer, the bandgap changes from indirect to direct at 8% (2%) of applied strain. In the β-P bilayer there also occurs a direct to indirect bandgap transition at e = 10%.

In all the considered hetero-bilayers, except γ-P/β-P, the bandgap first increases with the application of strain and then decreases and becomes less than 0.25 eV at 25% of strain (Fig. 6(b)). A closer examination at the band structure of all the hetero-bilayers shows that an initial increase in the bandgap with the application of strain is due to the simultaneous shift in the VBM and CBM away from the Fermi level. The decrease in the bandgap after attaining a maximum value is attributed to the simultaneous shift of the VBM and CBM towards the Fermi level. As a representative case, the band structure of α-P/β-P at various values of in-plane biaxial strain is given in Fig. S8 of the ESI.† The applied in-plane strain shifts the VBM and CBM, leading to the modification of the band gap, which is attributed to the redistribution of the out-of-plane atomic orbitals. In the γ-P/β-P bilayer, however, application of strain shifts the VBM and CBM towards the Fermi level until the bandgap reduces down to zero, producing metallization at 18% strain value. We have also found indirect-to-direct bandgap transition at 6% (10%) (10%) and then direct-to-indirect gap transition at 20% (16%) (18%) in α-P/β-P (γ-P/β-P) (δ-P/β-P) bilayers.

3.5. Effect of vertical pressure

In order to determine the effect of applied normal compression strain (e_z), we define it as $e_z = (R_0 - R)/R_0$, where R is the interlayer distance and R_0 is the equilibrium value of the interlayer distance. We decrease the interlayer distance of the bilayers, starting from the equilibrium value, in steps of 0.1 Å and calculate the corresponding normal compression strain (NCS) and bandgap. Fig. 7 shows the variation of the bandgap with NCS for all the considered systems. α-P, γ-P and δ-P bilayers show a negligible change in the bandgap up to e_z = 20%, 10% and 10% respectively, and after that the bandgap begins to reduce at a higher rate leading to semiconductor to metal transition at e_z = 39%, 20% and 21% respectively, for α-P, γ-P and δ-P bilayers. However, the bandgap reduces monotonically for β-P bilayers thus producing metallization at e_z = 34% (e_z = 38% for β-P in the rectangular unit cell). In the case of hetero-bilayers (except γ-P/δ-P), the bandgap remains constant up to 20% of strain. For e_z > 20% the bandgap reduces until metallization occurs at e_z = 39%. On the other hand, in the case of γ-P/δ-P, the applied NCS increases the bandgap. The band structures of α-P/β-P at different strain values as a representative case are shown in Fig. S9 of the ESI.† Although there is no significant change in the bandgap of α-P/β-P up to 20% strain (Fig. 7), the CBM continuously decreases to ∼20% and ∼79% of its initial values at 13.2% and 31.6% of applied strains respectively, while the VBM first increases to ∼14% and 22% of its initial values at 2.6% and 13.2% of strains respectively, and then at 21% of applied strain, the VBM is found to decrease

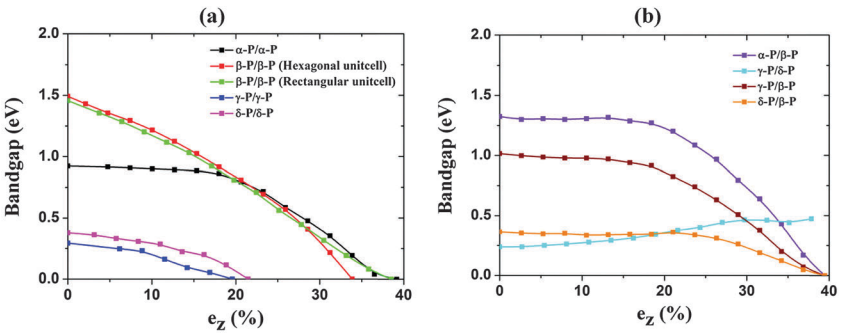

Fig. 7 Bandgap *vs.* applied normal compression strain (e_z) for (a) homo-bilayers and (b) hetero-bilayers of various structural phases of phosphorene.

by ~2% whereas at 31.6% of strain it decreases by ~56% of its equilibrium values.

Also in order to check the experimental feasibility of these NCS induced bandgap variations, we define pressure as the energy per unit area required to reduce the inter layer distance by $\Delta R = (R_0 - R)$, where R and R_0 are the strained and strain-free distances between the bilayers. Therefore, the applied pressure P is given by $(E - E_0)/((\Delta R) \times A)$, where E and E_0 are the strained and equilibrium bilayer energies, A is the area of the unit cell and ΔR is the change in the interlayer distance in moving from equilibrium to the strained configuration. Fig. 8 shows the variation of the fractional change in the bandgap with pressure for the considered homo- and hetero-bilayers.

It is found that applied pressure induces zero bandgap in all the homo- and hetero-bilayers (except γ-P/δ-P) *i.e.* in α-P/α-P (at 7.11 GPa), β-P/β-P (in the hexagonal unit cell at 4.77 GPa and in the rectangular unit cell at 5.81 GPa) (Fig. S10 of the ESI†), γ-P/γ-P (at 2.0 GPa), δ-P/δ-P (at 4.42 GPa), α-P/β-P (at 9.62 GPa), γ-P/β-P (at 8.18 GPa) and δ-P/β-P (at 11.34 GPa) (Fig. 8). But in the case of α-P/α-P, β-P/β-P, α-P/β-P, γ-P/β-P and δ-P/β-P the zero bandgap value occurs at the interlayer distances that approximately corresponds to the P–P bond length of phosphorene. Thus, the metallization in these cases is a result of covalent bonding between the corresponding layers of the bilayers. In the case of γ-P/γ-P and δ-P/δ-P complete semiconductor to metal transition occurs at a quite higher interlayer distance (3.0 Å). Applied normal compression strain also produces direct to indirect bandgap transition in α-P as well as in δ-P bilayers at an interlayer distance of 3.1 Å *i.e.*, at e_z = 18% and e_z = 19% respectively, corresponding to a pressure of 2.34 GPa in α-P and 3.63 GPa in δ-P. Among the hetero-bilayers, indirect to direct bandgap transition occurs in the case of the δ-P/β-P bilayer at e_z = 35.7% or at 5.28 GPa of pressure. The interlayer distance and the value of pressure at which metallization occurs for the considered systems are depicted in Table 3 and the magnitude of these pressure values indicate their experimental feasibility.

3.6. Effect of transverse electric field

Next we examine the effect of the external electric field on the electronic properties of the considered homo- and hetero-bilayer systems. The electric field is applied in the range from −1.0 V Å^{-1} to +1.0 V Å^{-1} in steps of 0.1 V Å^{-1}, in a direction perpendicular to the 2D structure. The positive direction of the electric field is taken along the positive z direction *i.e.*, from bottom towards the top layer, while the negative electric field is applied along the negative z-direction. Application of positive and negative electric fields shows an almost symmetric curve with respect to zero field axes for homo-bilayers (Fig. 9(a)) which is attributed to the homogeneity of atoms on the surface of both layers in the homo-bilayer system. The application of the electric field decreases the bandgap and produces metallization in α-P/α-P, γ-P/γ-P and δ-P/δ-P at ±0.7 V Å^{-1}, ±0.5 V Å^{-1} and ±0.5 V Å^{-1}, respectively. On the other hand, the bandgap gets reduced to ~28% of its initial value at ±1.0 V Å^{-1} for β-P/β-P (Fig. 9(a)).

Fig. 9(b) shows the variation of the bandgap in the case of hetero-bilayers with positive and negative transverse electric fields. The change in the bandgap of hetero-bilayers is not the same with positive and negative electric fields. As a representative case, the electronic band structure and isosurfaces of charge accumulation and charge depletion of the α-P/β-P hetero-bilayer in the presence of an applied positive and negative electric field is shown in Fig. S11 of the ESI.† The positive field shows the depletion of charge from the upper surface of the heterostructure while the negative field induces charge depletion from the lower surface of the hetero-bilayer. Both cases lead to the decrease in the band gap due to the accumulation of charge within the layers of heterostructures.

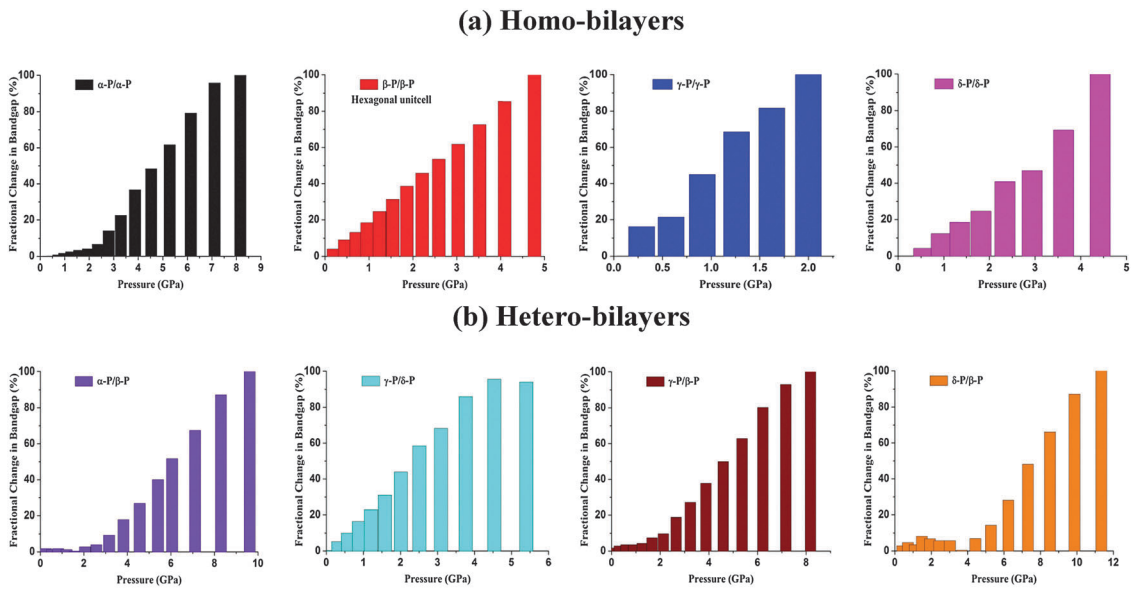

Fig. 8 The variation of the fractional change in the bandgap with pressure for (a) homo-bilayers and (b) hetero-bilayers of various structural phases of phosphorene.

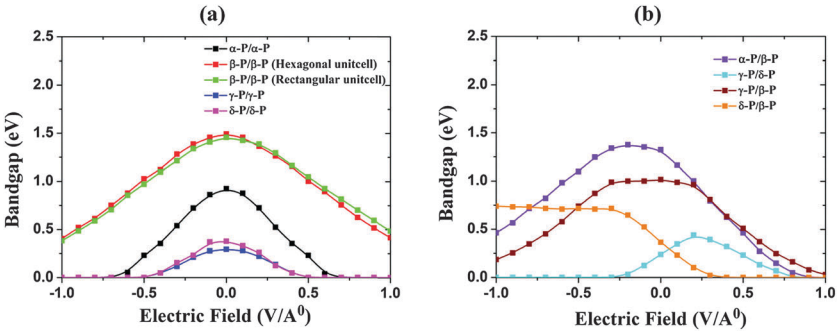

Fig. 9 The bandgap variation with the electric field for (a) homo-bilayers and (b) hetero-bilayers of various structural phases of phosphorene.

The application of the positive electric field decreases the bandgap linearly until metallization occurs at +0.9 V Å^{-1}, whereas with the negative electric field, the band structure shows a negligible change in the bandgap value up to −0.3 V Å^{-1}. The bandgap gets reduced upon further increase in the negative field. The different magnitude of the bandgap value with positive and negative fields is attributed to the counterbalance of the external electric field with an internal field induced due to the different structural phases and heterogeneity in the arrangements of atoms of each surface of the hetero-bilayer system. The complete metallization occurs at +0.9 V Å^{-1} for α-P/β-P, at −0.3 V Å^{-1} as well as +0.8 V Å^{-1} for γ-P/δ-P and at +0.4 V Å^{-1} for δ-P/β-P respectively, while γ-P/β-P remains a semiconductor for the considered range of applied electric fields with a bandgap value of 0.03 eV at +1.0 V Å^{-1} and 0.19 eV at −1.0 V Å^{-1}. Among all the bilayers, the electric field produces indirect to direct bandgap transition only in the δ-P/β-P bilayer at −0.3 V Å^{-1}.

4. Summary

Tuning of the electronic properties of homo- and hetero-bilayers of various structural phases of phospherene has been investigated within the DFT framework. Our total energy calculations reveal AB-stacking to be most favorable for the α-P bilayer while β-P, γ-P and δ-P bilayers prefer the AA-stacking pattern. All the homo-bilayers are found to be semiconducting. The γ-P homo-bilayer structure possess the highest UTS values *i.e.* 6.21 GPa and 4.47 GPa along *x* and *y* directions, while for the hetero-bilayer the UTS values are calculated to be in the range of 2.8–6.0 GPa. Both homo- and hetero-bilayers show a significant modulation of the bandgap upon application of in-plane tensile strain. A transition from semiconductor to metal has been found to occur at a critical value of transverse pressure. The modulation of the bandgap strongly depends on the polarity of the external electric field for hetero-bilayers, due to different structural phases and heterogeneity in the arrangement of atoms on each surface of the bilayer system. Electronic structure engineering by mechanical strain, pressure and transverse electric field in homo- and hetero-bilayers of various structural phases of phosphorene may be useful to fabricate next generation devices based on van der Waals bilayer structures.

References

1 A. K. Geim and K. S. Novoselov, The Rise of Graphene, *Nat. Mater.*, 2007, **6**, 183.
2 S. Z. Butler, S. M. Hollen, L. Cao, Y. Cui, J. A. Gupta, H. R. Gutiérrez, F. T. Heinz, S. S. Hong, J. Huang, A. F. Ismach, E. Johnston-Halperin, M. Kuno, V. V. Plashnitsa, R. D. Robinson, R. S. Ruoff, S. Salahuddin, J. Shan, L. Shi, M. G. Spencer, M. Terrones, W. Windl and J. E. Goldberger, Progress, Challenges, and Opportunities in Two-Dimensional Materials Beyond Graphene, *ACS Nano*, 2013, **7**, 2898.
3 H. Wang, H. Yuan, S. S. Hong, Y. Li and Y. Cui, Physical and Chemical Tuning of Two dimensional Transition Metal Dichalcogenides, *Chem. Soc. Rev.*, 2015, **44**, 2664.
4 Q. H. Wang, K. Kalantar-Zadeh, A. Kis, J. N. Coleman and M. S. Strano, Electronics and Optoelectronics of Two-dimensional Transition Metal Dichalcogenides, *Nat. Nanotechnol.*, 2012, **7**, 699.
5 J. Wu, B. Wang, Y. Wei, R. Yang and M. Dresselhaus, Mechanics and Tunable Bandgap by Straining in Single-Layer Hexagonal Boron-Nitride, *Mater. Res. Lett.*, 2013, **1**, 200.
6 H. Oughaddou, H. Enriquez, M. R. Tchalala, H. Yildirim, A. J. Mayne, A. Bendounan, G. Dujardin, M. A. Ali and A. Kara, Silicene, a promising new 2D material, *Prog. Surf. Sci.*, 2015, **90**, 46.
7 J. R. Brent, N. Savjani, E. Lewis, S. Haigh, D. Lewis and P. O'Brien, Production of few-layered phosphorene by liquid exfoliation of black phosphorous, *Chem. Commun.*, 2014, **50**, 13338.
8 S. Das, W. Zhang, M. Demateau, A. Hoffmann, M. Dubey and A. Roelofs, Tunable Transport Gap in Phosphorene, *Nano Lett.*, 2014, **14**, 5733.
9 L. Li, Y. Yu, G. J. Ye, Q. Ge, X. Ou, H. Wu, D. Feng, X. H. Chen and Y. Zhang, Black Phosphorus Field-effect Transistors, *Nat. Nanotechnol.*, 2014, **9**, 372.
10 F. Xia, H. Wang and Y. Jia, Rediscovering Black Phosphorus as an Anisotropic Layered Material for Optoelectronics and Electronics, *Nat. Commun.*, 2014, **5**, 4458.
11 Y. Cai, Q. Ke, G. Zhang, Y. P. Feng, V. B. Shenoy and Y.-W. Zhang, Giant Phononic Anisotropy and Unusual Anharmonicity of Phosphorene: Interlayer Coupling and Strain Engineering, *Adv. Funct. Mater.*, 2015, **25**, 2230–2236.

12 Z. Zhu and D. Tománek, Semiconducting Layered Blue Phosphorus: A Computational Study, *Phys. Rev. Lett.*, 2014, **112**, 176802.
13 J. Guan, Z. Zhu and D. Tománek, Phase coexistence and metal insulator transition in few-layer phosphorene: A computational study, *Phys. Rev. Lett.*, 2014, **113**, 046804.
14 S. E. Boulfelfel, G. Seifert, Y. Grin and S. Leoni, Squeezing lone pairs: The A17 to A7 pressure-induced phase transition in black phosphorus, *Phys. Rev. B: Condens. Matter Mater. Phys.*, 2012, **85**, 014110.
15 M. Wu, H. Fu, L. Zhou, K. Yao and X. C. Zeng, Nine New Phosphorene Polymorphs with Non-Honeycomb Structures: A Much Extended Family, *Nano Lett.*, 2015, **15**, 3557.
16 L. Kou, C. Chen and S. C. Smith, Phosphorene: Fabrication, Properties, and Applications, *J. Phys. Chem. Lett.*, 2015, **6**, 2794–2805.
17 J. B. Smith, D. Hagaman and H.-F. Ji, Growth of 2D black phosphorus film from chemical vapor deposition, *Nanotechnology*, 2016, **27**, 215602.
18 T. Niu and A. Li, From two-dimensional materials to heterostructures, *Prog. Surf. Sci.*, 2015, **90**, 21.
19 M. Li, C. Chen, Y. Shi and L. Li, Heterostructures based on two-dimensional layered materials and their potential applications, *Mater. Today*, 2015, 1.
20 P. Rivero, C. M. Horvath, Z. Zhu, J. Guan, D. Tománek and S. Barraza-Lopez, Simulated scanning tunneling microscopy images of few-layer phosphorene capped by graphene and hexagonal boron nitride monolayers, *Phys. Rev. B: Condens. Matter Mater. Phys.*, 2015, **91**, 115413.
21 J. E. Padilha, A. Fazzio and A. J. R. da Silva, van der Waals Heterostructure of Phosphorene and Graphene: Tuning the Schottky Barrier and Doping by Electrostatic Gating, *Phys. Rev. Lett.*, 2015, **114**, 066803.
22 G.-C. Guo, D. Wang, X.-L. Wei, Q. Zhang, H. Liu, W.-M. Lau and L.-M. Liu, First-Principles Study of Phosphorene and Graphene Heterostructures Anode Materials for Rechargeable Li Batteries, *J. Phys. Chem. Lett.*, 2015, **6**, 5002.
23 Y. Cai, G. Zhang and Y.-W. Zhang, Electronic Properties of Phosphorene/Graphene and Phosphorene/Hexagonal Boron Nitride Heterostructures, *J. Phys. Chem. C*, 2015, **119**, 13929–13936.
24 Y. Deng, Z. Luo, N. J. Conrad, H. Liu, Y. Gong, S. Najmaei, P. M. Ajayan, J. Lou, X. Xu and P. D. Ye, Black Phosphorus Monolayer/MoS_2 van der Waals Heterojunction p–n Diode, *ACS Nano*, 2014, **8**, 8292.
25 H. Liu, A. T. Neal, Z. Zhu, Z. Luo, X. Xu, D. Tománek and P. D. Ye, Phosphorene: An Unexplored 2D Semiconductor with a High Hole Mobility, *ACS Nano*, 2014, **8**, 4033–4041.
26 K. Gong, L. Zhang, W. Ji and H. Guo, Electrical contacts to monolayer black phosphorus: A first-principles investigation, *Phys. Rev. B: Condens. Matter Mater. Phys.*, 2014, **90**, 125441.
27 X. Peng, Q. Wei and A. Copple, Strain-engineered direct-indirect bandgap transition and its mechanism in two-dimensional phosphorene, *Phys. Rev. B: Condens. Matter Mater. Phys.*, 2014, **90**, 085402.
28 M. Sharma, A. Kumar, P. K. Ahluwalia and R. Pandey, Strain and electric field induced electronic properties of two-dimensional hybrid bilayers of transition-metal dichalcogenides, *J. Appl. Phys.*, 2014, **116**, 063711.
29 A. Kumar, H. He, R. Pandey, P. K. Ahluwalia and K. Tankeshwar, Pressure and electric field-induced metallization in the phase-engineered ZrX_2 (X = S, Se, Te) bilayers, *Phys. Chem. Chem. Phys.*, 2015, **17**, 19215.
30 R. Fei and L. Yang, Lattice vibrational modes and Raman scattering spectra of strained phosphorene, *Appl. Phys. Lett.*, 2014, **105**, 083120.
31 M. Buscema, D. J. Groenendijk, S. I. Blanter, G. A. Steele, H. S. J. vanderZant and A. Castellanos-Gomez, Fast and Broadband Photoresponse of Few-Layer Black Phosphorus Field-Effect Transistors, *Nano Lett.*, 2014, **14**, 3347.
32 S. Liu, N. Huo, S. Gan, Y. Li, Z. Wei, B. Huang, J. Liu, J. Li and H. Chen, Thickness-dependent Raman spectra, transport properties and infrared photoresponse in few-layer black phosphorus, *J. Mater. Chem. C*, 2015, **3**, 10974.
33 H. Y. Lv, W. J. Lu, D. F. Shao and Y. P. Sun, Enhanced thermoelectric performance of phosphorene by strain-induced band convergence, *Phys. Rev. B: Condens. Matter Mater. Phys.*, 2014, **90**, 085433.
34 R. Fei, A. Faghaninia, R. Soklaski, J.-A. Yan, C. Lo and L. Yang, Enhanced Thermoelectric Efficiency via Orthogonal Electrical and Thermal Conductances in Phosphorene, *Nano Lett.*, 2014, **14**, 6393.
35 L. Kou, T. Frauenheim and C. Chen, Phosphorene as a Superior Gas Sensor: Selective Adsorption and Distinct I–V Response, *J. Phys. Chem. Lett.*, 2014, **5**, 2675.
36 W. Li, Y. Yang, G. Zhang and Y.-W. Zhang, Ultrafast and Directional Diffusion of Lithium in Phosphorene for High-Performance Lithium-Ion Battery, *Nano Lett.*, 2015, **15**, 1691.
37 J. M. Soler, E. Artacho, J. D. Gale, A. Garcia, J. Junquera, P. Ordejon and D. S. Portal, The SIESTA method for ab initio order-N Materials Simulation, *J. Phys.: Condens. Matter*, 2002, **14**, 2745.
38 N. Troullier and J. L. Martins, Efficient Pseudopotentials for Plane-Wave Calculations, *Phys. Rev. B: Condens. Matter Mater. Phys.*, 1991, **43**, 1993.
39 M. Dion, H. Rydberg, E. Schröder, D. C. Langreth and B. I. Lundqvist, Van der Waals Density Functional for General Geometries, *Phys. Rev. Lett.*, 2004, **92**, 246401.
40 J. Dai and X. C. Zeng, Bilayer Phosphorene: Effect of Stacking Order on Bandgap and Its Potential Applications in Thin-Film Solar Cells, *J. Phys. Chem. Lett.*, 2014, **5**, 1289.
41 B. Ghosh, S. Nahas, S. Bhowmick and A. Agarwal, Electric field induced gap modification in ultrathin blue phosphorus, *Phys. Rev. B: Condens. Matter Mater. Phys.*, 2015, **91**, 115433.
42 Y. Cai, G. Zhang and Y.-W. Zhang, Layer-dependent Band Alignment and Work Function of Few-Layer Phosphorene, *Sci. Rep.*, 2014, **4**, 6677.

43 Q. Liu, X. Zhang, L. B. Abdalla, A. Fazzio and A. Zunger, Switching a Normal Insulator into a Topological Insulator via Electric Field with Application to Phosphorene, *Nano Lett.*, 2015, **15**, 1222.
44 Y. Li and X. Chen, Dirac Fermions in Blue-Phosphorus, *2D Mater.*, 2014, **1**, 031002.
45 M. Wu, X. Qian and J. Li, Tunable Exciton Funnel Using Moiré Superlattice in Twisted van der Waals Bilayer, *Nano Lett.*, 2014, **14**, 5350.
46 A. Kumar and P. K. Ahluwalia, Mechanical strain dependent electronic and dielectric properties of two-dimensional honeycomb structures of MoS_2 (X = S, Se, Te), *Phys. B*, 2013, **419**, 66.

